Spatially-resolved magnetic resonance study of the dissolution interface between soaps and water

E Ciampi[1], **U Goerke**[1], **P J McDonald**[1], **J G Chambers**[2] **and B Newling**[2,3,4]

[1] Department of Physics, School of Physics and Chemistry, University of Surrey, Guildford, GU2 7XH, UK

[2] Unilever Research Port Sunlight, Quarry Road East, Bebington, Wirral, CH63 3JW, UK

E-mail: bnewling@unb.ca

Abstract

The developing interfacial region between a soap bar and water has been studied using a suite of spatially resolved NMR techniques. Stray field imaging (STRAFI) allowed the dynamics of water ingress into a shop-bought, commercial soap to be followed. A simplistic analysis of the data shows the ingress to be a Fickian process ($\propto t^{1/2}$) in the first 4 h. The T_2 contrast employed in the STRAFI method is not sufficient to resolve detail of the mesophase formation at the interface. However, double quantum filtered ^{2}H spectroscopy at different positions in the interfacial region allowed water concentration (and mesophase distribution) to be mapped over the first 120 h of dissolution. A simple model shows good agreement with the water concentration data. In the isotropic soap solution above the interfacial region, J-cyclic cross polarization was used to selectively interrogate the CH$_2$ ^{1}H of the soap alkyl chains and, in combination with a pulsed field gradient measurement of self-diffusion, suggests a micellar solution in which the hydrodynamic radius of the micelles is $\sim$5 nm.

1. Introduction

The spontaneous formation of lyotropic mesophases at the interface between some solid materials and water is a property used to advantage for controlled release [1]. The mesophases, some with very high viscosity, form a barrier to water penetration. This process is also critical in determining the in-use properties of structured surfactant products, such as soap bars and detergent powders, whose rate of dissolution can similarly be governed by the formation of mesophases at their solid–liquid interface. However, in spite of the ubiquity of such products, surprisingly little is known about the spatial development of these mesophases. Knowledge of the water concentration gradient and mesophase structure across the developing interface is required to facilitate the improvement of the processing, formulation and in-use properties of surfactant products.

One possible methodology for studying mesophases is optically polarized light microscopy [2, 3]. The mesophases have characteristic optical textures that can be used to identify their structure. However, commercial soap formulations also contain solid re-crystallized components, which are birefringent. These are difficult to distinguish from the mesophase and hence mask detail. An alternative technique is nuclear magnetic resonance (NMR) which is able to provide information about both structure and dynamics at the molecular level. NMR, in one form or another, has proved an invaluable tool in the study of mesophase formation and properties in the bulk: spectroscopy [4, 5], relaxation analysis [5, 6] and diffusometry [7, 8] have all been used successfully. The use of magnetic resonance imaging (MRI) for the spatially resolved study of solid–liquid interfacial regions follows as a natural consequence. MRI is both non-invasive and non-destructive.

---

[3] Author to whom correspondence should be addressed.
[4] Current address: Department of Physics, University of New Brunswick, PO Box 4400, Fredericton, NB, Canada E3B 5A3.

In this paper we present a study of the interface between a soap bar and water using a suite of spatially resolved NMR techniques. We seek to explore the capabilities of these techniques for both a model and a commercial formulation with the specific objective of determining a space–time map of the mesophase structure in the interface layer.

The soap bar itself contains several, different phases with different NMR relaxation properties, because there is a heterogeneous microscopic distribution of water throughout the bar. Low water domains (solid soap, for example) coexist with higher water domains (such as lyotropic mesophases). One model of soap bar structure envisages the viscous mesophase domains as a glue, which hold domains with lower water contents together. These domains are in general too small to be individually visible to conventional MRI techniques, due to the mixing regimes of soap bar manufacture. At the interface between a soap bar and water, however, a gradient of water concentration develops. The interface region will therefore again contain a spatial distribution of phases from the soap/water phase diagram, but on a larger scale than within the bar. T_2 contrast is inherent to the interface due to the different relaxation properties of the different phases.

Spatial resolution of the different phases in the interfacial bar/water region is, in principle, possible by virtue of their different T_2 values alone. However, the short T_2 components are invisible to conventional MR microscopy methods, as application of an imaging pulse sequence generally takes on the order of milliseconds to allow time for gradient switching. We present a stray field imaging (STRAFI) study of the developing interfacial region. The STRAFI technique is performed in a permanent magnetic field gradient, which allows rapid signal acquisition. Short and long T_2 components both contribute to the STRAFI signal. The STRAFI measurements allowed some quantification of the dissolution process based on T_2 contrast, but failed to reveal any detail of the mesophase distribution at the interface (see section 4).

A more sophisticated contrast was developed when the interfacial region between a soap bar and heavy water (^2H_2O) was studied. Use of a double quantum filter (DQF) allowed suppression of signal from isotropic ^2H-containing solution and, thereby, mapping of the mesophase distribution at the interface.

Finally, cyclic J-cross polarization (CYCLCROP) was used to study the isotropic solution above the soap/water interface. The technique suppressed the water signal and selectively interrogated the CH_2 ^1H in the soap solution. CYCLCROP was combined with a pulsed field gradient (PFG) pulse sequence to observe the self-diffusion behaviour of the soap alkyl chains in solution, from which information about the microstructure of the solution could be deduced.

2. Materials

A variety of soap bars was studied. All contained mixtures of surfactants. STRAFI measurements were performed on a cylindrical core, taken from a shop-bought, commercial soap bar (*Pears*), which was pressed into a glass tube. Relaxometry and ^2H measurements were made, for the most part, on a model soap mixture (80/20 animal soaps/vegetable soaps) with a moisture content of about 14 wt% with occasional repeats on

a commercial soap formulation (moisture content $\sim$13 wt%). The latter was identical in composition to the model soap except for the addition of preservative, perfume and colouring. Equilibrated soap/water mixtures (see figure 3) were prepared by weighing the required quantities of soap and ^2H_2O into a glass vessel and heating to 90°C for 24 h with occasional stirring. Two methods of preparation were used to study the interfacial soap/water region. In the first, cylinders of soap were cored directly into glass tubing to fill about half of the tube length of 10 cm. In the second method, soap was extruded from a plastometer directly into the tubing. The choice of sample preparation had no appreciable effect upon the results, provided the soap samples were taken from fresh soap. Water or ^2H_2O was added into the empty half of the tube in order for the interfacial region to develop. This choice of sample geometry allowed the development of a soap/water interfacial region to be treated as a one-dimensional problem (neglecting any effect of the glass/soap interface upon the soap/water interaction).

3. Methods

^1H NMR T_2 relaxometry on the soap bars was performed at 20 MHz in a QP20+ benchtop spectrometer (Oxford Instruments, Oxon, UK). All other NMR experiments were carried out on a 400 ^1H MHz Chemagnetics Infinity Spectrometer (Varian Solid State Office, UK), coupled to a Magnex 9.0 T superconducting magnet (Magnex, Oxon, UK). A homebuilt probe assembly was used to acquire STRAFI data and a homebuilt, variable temperature, ^2H probehead was used for the acquisition of ^2H data. A doubly tuned ^{13}C–^1H probehead (IBMT, Frauenhofer Institute, Germany) was used to acquire CYCLCROP data and a ^1H microscopy probe from the same manufacturer was used for ^1H imaging. The imaging gradients and Matrix Shim Set were supplied by Resonance Research Instruments, USA.

3.1. Relaxometry

Two relaxation decays were acquired for each soap sample: a free induction decay (FID) and a Carr–Purcell–Meiboom–Gill (CPMG) decay [9]. The FID was acquired following a single radio frequency (RF) excitation pulse using a dwell time of 1 μs and total acquisition time of 1 ms. The acquired signal-to-noise ratio exceeded 1000. The CPMG decay consisted of 24 echoes separated by 800 μs. The signal-to-noise ratio exceeded 400. The 90° excitation pulse length was 2.5 μs. T_2 relaxation components were calculated using a gradient expansion algorithm to compute a non-linear least squares fit to NMR decays [10] in the IDL software suite (Research Systems Inc., Colorado, USA).

3.2. PFG measurements of self-diffusion

Self-diffusion-weighted spectra were acquired using the stimulated-echo variant of the PFG spin-echo technique [11, 12]. The pulse sequence is defined in figure 1(*a*). Following excitation of the nuclear spin magnetization by a 90° RF pulse, a magnetic field gradient g of duration δ is applied. The gradient imposes a precessional phase shift on the nuclear
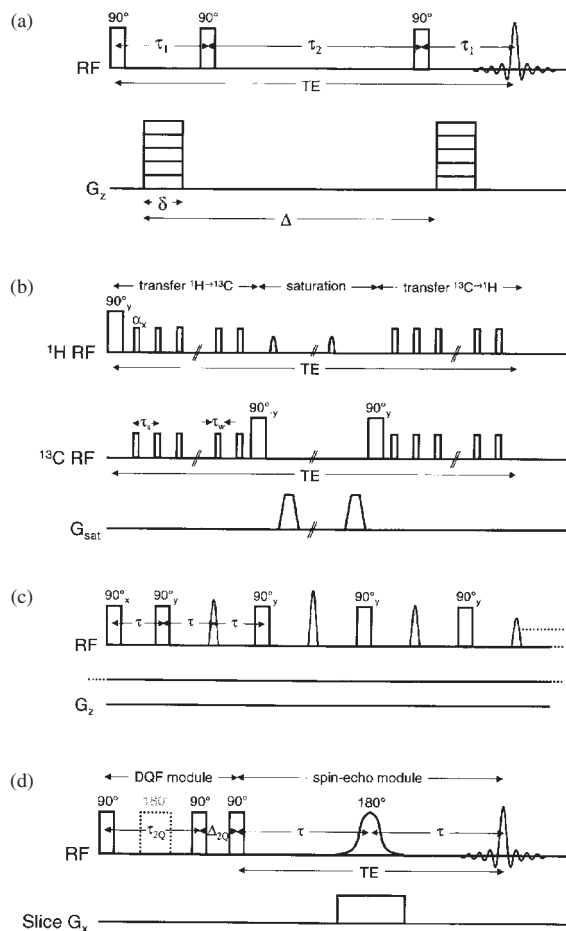
Figure 1. (*a*) Pulse sequence timing diagram for PFG spin-echo measurements of spectral attenuation caused by self-diffusion. The upper line (RF) shows the sequence of radiofrequency excitation and detection, the lower line (G_z) indicates the sequence of concurrent magnetic field gradient application. The PFGs are incremented in a series of repeats of the whole timing diagram. Fourier transformation of the echo signals, collected at time TE, yields a series of NMR spectra sensitized to self-diffusion by the gradient application. (*b*) Pulse sequence for the CYCLCROP preparation module. (*c*) Multiple quadrature echo pulse sequence used in the STRAFI profiling. The magnetic field gradient (G_z) is due to the field inhomogeneity in the fringe field of the magnet and is, therefore, present throughout the measurement. (*d*) Pulse sequence for slice-selective DQF spectroscopy.

spins, which depends upon position. It is followed, at time τ_1 after the first 90° pulse, by a second 90° pulse, which stores the magnetization along the z-axis of the static polarizing field for a period τ_2. The stored magnetization is recalled by a third 90° pulse, whereupon a second gradient pulse g is applied which imposes a reversed phase shift. An echo signal is formed, the magnitude of which is dependent on diffusion during the diffusion time Δ according to

$$\frac{A}{A_0} = \exp\left(-(\gamma \delta g)^2 D_{\text{self}}\left(\Delta - \frac{\delta}{3}\right)\right), \qquad (1)$$

where A is the signal echo (or echo Fourier component) amplitude, A_0 is the amplitude when $g = 0$ and γ is the magnetogyric ratio for the investigated nuclei. Other parameters are defined in the figure. The self-diffusion

coefficient D_{self} is extracted from the fit to the data. In the work reported here measurements were made as a function of g with timing parameters (δ, Δ) kept constant. Typical parameters used for ^{1}H were $\delta = 2$ ms, $\Delta = 10$ ms although, in some cases, Δ was increased up to 600 ms.

Indirectly detected ^{13}C self-diffusion spectra were obtained using CYCLCROP [13] weighted PFG sequences. The CYCLCROP module replaces the first excitation pulse of the PFG sequence. The chemical selectivity of the CYCLCROP module is used to detect hydrogen resonances associated with specific ^{13}C^{1}H$_n$ units: here the methylene ^{13}C^{1}H$_2$ in mobile soap molecules. The method excites all ^{1}H magnetization, transferring this to ^{13}C at the chosen sites, stores all of the selected magnetization on ^{13}C during destruction of unwanted ^{1}H magnetization and transfers the selected magnetization back from ^{13}C to ^{1}H (figure 1(*b*)). The so-called PRAWN variant, which is well described in the literature [14], was used in the cross-coupling to ^{13}C and consisted of 15 coupling pulses of nominal flip angle 24° applied over 4.5 ms. The saturation scheme consisted of four adiabatic half passages, each 6 ms long, with the frequency set on the water signal, in combination with field gradient pulses.

3.3. ^{1}H Imaging

MR micrographs of mobile ^{1}H components in a dissolving soap section were obtained using a standard spin-echo imaging sequence comprising slice selection and phase and frequency spatial encoding of a spin echo [12]. The slice thickness was typically 2 mm and the in-plane pixel resolution 39 μm × 625 μm. The chosen echo time was generally 4 ms. For the most part, 32 acquisitions were co-added over 17 min to form each image. Standard Fourier processing was applied.

STRAFI was used to map less mobile components in one dimension, along the sample length. STRAFI is a sensitive plane technique which is carried out in the fringe field of a superconducting magnet [15–17]. It is one of a class of techniques, others including SPRITE [18] and Gradient echo [19], developed for, and applicable to, broad-line systems. The field strength at the sample position in the fringe field of the Magnex magnet was 5.5 T and the constant gradient strength was 58 T m^{-1}. Under these conditions, a 10 μs RF pulse excites only a narrow slice of the sample, about 40 μm in thickness, at the centre of the RF sensor coil. A profile of the sample is built up by investigating that sensitive slice and then moving the sample (using a homebuilt stepper motor assembly) to permit investigation of the next slice. The pulse sequence used at each location was the multiple quadrature echo sequence shown in figure 1(*c*). The sequence consists of a 90° RF pulse followed by a train of n phase shifted pulses, each yielding an echo signal. Typically in the work reported here, $n = 128$ echoes were generated and the basic pulse gap, τ, was 22.5 μs; complete profiles were acquired every 6 min for 2 h and thereafter every 12 min.

3.4. ^{2}H and DQF spectroscopy and imaging

The anisotropic environment of deuterated water in liquid crystalline phases gives rise to a non-zero, residual electric quadrupole energy level splitting for the deuterium nuclei, which manifests as a splitting of the spectral line for ^{2}H$_2$O

1273

in the liquid crystal phase. The ^{2}H spectrum of mixed liquid crystal and isotropic solution is a superposition of the liquid crystal doublet and the isotropic singlet. The double quantum signal associated with anisotropic liquid crystal can be separated from isotropic solution by suppressing the isotropic solution signal, in a process known as DQF.

The basic DQF sequence which is shown in the first part of figure 1(d) is a routine tool in high-resolution NMR spectroscopy [20]. It consists of three 90° RF pulses. The first creates single quantum coherences, which are observable in the form of transverse magnetization. With time, these evolve into a mixture of one and two spin single quantum coherences. At time τ_{2Q} after the first pulse, a second pulse is applied which creates double quantum coherences. The third pulse recovers the magnetization to observable single quantum coherence. The purpose of the second and third pulses is to eliminate, by phase cycling, unwanted single quantum coherences so that, on completion of the phase cycle, only signal from deuterium in anisotropic environments is observed and, in the spectra, is manifest as a characteristic doublet with one positive and one negative peak separated by the quadrupolar splitting. A 180° pulse is often inserted in the middle of the τ_{2Q} interval to refocus chemical shift and inhomogeneous magnetic field interactions. Spatially localized ^{2}H DQF spectra from narrow slices at different positions along the length of dissolving solid soap were recorded by replacing the first, non-selective 90° pulse of a spin-echo sequence with the DQF module. The frequency selective 180° pulse of the spin-echo sequence was made slice selective by simultaneous gradient application. In the experiments reported here, τ_{2Q} was 1.1 ms.

4. Results and discussion

4.1. Relaxometry

The distribution of T_2 relaxation time constants determined from FID and CPMG echo-train decays of the model soap bar at two temperatures, 20 and 40°C are presented in table 1. The errors quoted are the statistical standard error arising from analysis of repeated measurements on a commercial *Pears* soap bar at 29°C. The data analysis assumes a total of four relaxation components. The FID was fit to a Gaussian decay ($T_2 \approx 10\,\mu$s) representing the various solid soap phases, a short T_2 exponential decay ($T_2 \approx 100\,\mu$s) ascribed to the liquid crystal phases and a longer component attenuated by magnetic field inhomogeneities. This final component overlaps with, and is better measured in, the CPMG experiment. The CPMG decays have been fit to two component exponential decays with intermediate ($\sim$1 ms)

and long ($\sim$10 ms) time constant decays, respectively. Both components are essentially liquid in character. Previous measurements of the T_2 distribution in a pure hexagonal liquid crystal phase [21], comprising the soluble soap components of the model used here, show three components, which correspond to the $\sim$100 μs component and two exponential components of the CPMG decay. The results in table 1 are, therefore, consistent with a bar containing solid soap and a hexagonal liquid crystalline phase, in which the liquid components ($\sim$1 and 10 ms) are a part of the liquid crystal phase. The results are typical of many soap formulations studied in our laboratories.

The partition of a FID and CPMG echo train into four components is notoriously difficult and unreliable. However, in the present case we believe the procedure to be justified. The four-time constants all differ by about an order of magnitude and are of significant amplitude—often considered to be necessary for their distinction to be valid [22]. The component with overall smallest fraction (intermediate $\sim$1 ms, 7% at 20°C) has an amplitude in excess of 10% of the largest (solid soap, 61% at 20°C). Excluding the solid soap, which in many ways is the easiest to identify, the remaining three are of comparable amplitude. From known phase chemistry, there is reason to believe that four components are possible in this discretized model [23]. It is well known that water closely associated with surfactant headgroups and water in the layers between those surface layers have different values of relaxation time constants [24] and that the rapid exchange of water molecules between those two environments leads to an averaged value of T_2 which depends upon the water content of the liquid crystal domains. In the heterogeneous soap bar sample, a distribution of water contents in liquid crystalline domains contributes to the resolution of two components. The total proportions of liquid components suggest that the surfactant molecules themselves also contribute to a certain extent. While the multiple components (particularly those due to the water) would undoubtedly be better represented by a continuous distribution of T_2 values, the analysis performed is entirely adequate to characterize the material and to indicate the echo time windows available to visualize different components in imaging experiments.

The primary changes induced by an increase in temperature are a melting of solid soap into the liquid crystal phase and an increase in the mobility of the shorter liquid component. Increased diffusive attenuation may account for the decrease in the apparent T_2 of the mobile isotropic solution, but the increase in proportion of liquid crystal phase at fixed water concentration will also form some liquid crystal domains with smaller inter-headgroup spacings and, hence, shorter T_2. These results are also typical of many soap formulations.

Table 1. The T_2 relaxation distribution of model soap at 20°C and 40°C.

Component	Soap (20°C)		Soap (40°C)	
	Relative fraction (%)	T_2 (ms)	Relative fraction (%)	T_2 (ms)
Solid soap	61 ± 1	$0.011 \pm <0.001$	56 ± 1	$0.012 \pm <0.001$
Liquid crystal	17.3 ± 0.5	0.088 ± 0.001	20.7 ± 0.5	0.095 ± 0.001
Liquid (intermediate) in liquid crystal	7.0 ± 0.2	0.87 ± 0.08	7.0 ± 0.2	1.55 ± 0.08
Liquid (long) in liquid crystal	15 ± 1	18.4 ± 0.2	16 ± 1	13.8 ± 0.2

4.2. Spectroscopy of equilibrated solutions

Figure 2 shows the variation in quadrupolar splitting for ^{2}H spectra of equilibrated soap solutions at 60°C. The equilibrated samples were prepared from the model soap. No quadrupolar splitting was observed above 73% water concentration indicating that no mesophases were present. It is therefore concluded that the solution is isotropic in this range.

Between 50% and 73% water concentration, powder-like quadrupolar spectra were observed, such as in the lower spectrum of figure 2. It is inferred that ^{2}H$_2$O molecules and mesophase domains in these equilibrium samples were randomly oriented with respect to the applied magnetic field and that the domains did not reorient during the course of the NMR measurement due to the viscosity of the sample. The values of $\Delta\nu_q$ were measured between the inner (major) peaks of the powder spectrum. This splitting arises from those surfactant aggregates with symmetry axis orthogonal to the main magnetic field. Further measurements would be required to determine the orientation of the solvent molecules with respect to the mesophase domains and, hence, the orientation of the optical mesophase director with respect to the magnetic field. The splitting increased from 0.1 to 0.5 kHz as the water concentration was decreased, a behaviour which is typical of liquid crystalline mesophase [25].

Samples in which the water concentrations was in the approximate range 30–50% initially gave a single, very broad resonance. After several hours in the magnetic field and some *in situ* temperature cycling up to 110°C, the mesophase domains became oriented with respect to the magnetic field and gave two pairs of narrow lines such as those in the upper spectrum of figure 2. The two well-resolved values of $\Delta\nu_q$ for these spectra were straightforwardly extracted. The smaller of the splittings was very similar to that observed at higher water concentrations. The additional splitting was much greater, 1–2 kHz. The splittings again increased as the water concentration decreased. It is likely that a hexagonal liquid crystalline mesophase (rod-shaped soap aggregates) is responsible for the smaller splitting and that a lamellar liquid crystalline mesophase (soap bilayers) gives rise to the larger splitting. The presence of both phases is probably due to some residual heterogeneity of water content in the sample, which is an indication of the difficulties of preparing equilibrated
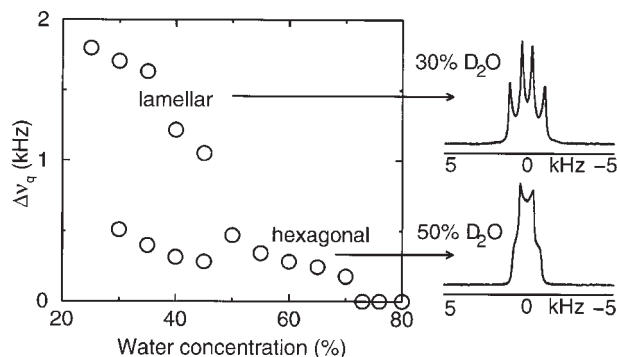
samples at very low water contents (with high viscosity). This hypothesis is consistent with a general binary phase diagram for a single soap and water [23].

By 25% water concentration no hexagonal (small splitting) phase remains and the only mesophase present is lamellar. Additionally, there is a broad ^{2}H line (half height linewidth $\sim$120 Hz), the origin of which is unclear: there is some possibility of ^{1}H$\leftrightarrow^2$H exchange between water (H$_2$O) in the soap and ^{2}H$_2$O at 90°C leading to a broad ^{2}H line for the solid soap. There is no evidence for a soap $\Delta\nu_q$ at higher water concentrations. It was not possible to make macroscopically homogeneous solutions at still lower water concentrations. The measurements were repeated for the commercial formulation containing perfume and colouring. The results were essentially unchanged.

4.3. Measurements of self-diffusion

The first measurements of self-diffusion presented are of the water in an isotropic soap solutions at 60°C and 90% water concentration. In this solution the water and primary soap resonances were well resolved in the NMR spectrum and their attenuation under the PFGs was readily measured. The signal attenuation with gradient strength for the water resonance was well represented by equation (1). The diffusion coefficient calculated from the fit was 4.7×10^{-9} m^2 s^{-1}. The measured values are in good agreement with literature values for water at 60°C [26]. The soap resonance decay was less well represented by the single exponential of equation (1). Rather it was found that a linear combination of two exponentials gave a much improved fit. An example data set and fitting is shown in the lower graph of figure 3. The two components occurred
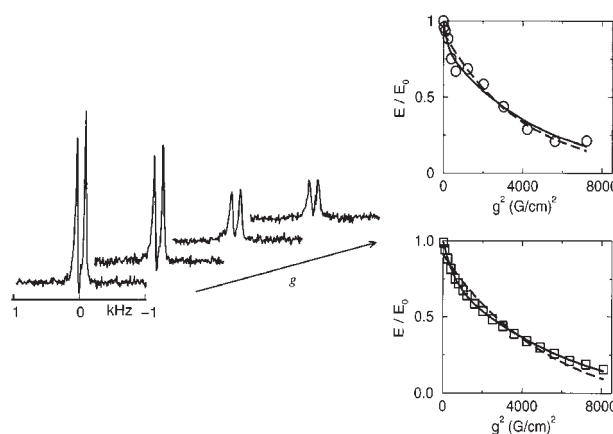

Figure 3. Four CYCLCROP ^{13}C-edited PFG spectra acquired with increasing amplitudes of pulsed magnetic field gradient (g increases in the direction of the arrow). The CYCLCROP preparation ensures that the spectra contain only signal from the protons in –CH$_2$– groups, signal from water is completely suppressed. The upper graph shows the attenuation with g^2 of the dominant (soap) peak in spectra such as these. The data are well represented by a two component (biexponential) fit, which is plotted as a solid line. A single component fit (- - - -) is a poorer representation of the data. The lower graph shows attenuation of the soap signal obtained without CYCLCROP editing, in which the soap and water signals are separated by relying only upon chemical shift dispersion. The signal-to-noise per unit time is better for these than for the CYCLCROP data and the two-component fit (———) is again better than a single component.

Figure 2. Variation in measured quadrupolar splitting for ^{2}H spectra of equilibrated model soap/^{2}H$_2$O samples at 60°C (see text for details of preparation). The insets show examples of the spectra from which these data were taken. The ^{2}H$_2$O concentration for these spectra were 30% (top) and 50% (bottom).

in the intensity ratio 20:80 with diffusion coefficients of $(3.0 \pm 0.1) \times 10^{-9} \, \text{m}^2 \, \text{s}^{-1}$ and $(1.0 \pm 0.1) \times 10^{-10} \, \text{m}^2 \, \text{s}^{-1}$. The slower component is a measure of soap micellar diffusion. Individual soap molecules move into and out of micelles on a timescale far shorter than the duration of the NMR measurement [27] so the measured micellar diffusion is an average of the diffusion coefficient of a soap micelle and the diffusion coefficient of an isolated soap molecule in solution, weighted by the proportions of soap molecules in these two states. Assuming that the majority of the soap molecules present are in micelles (a 10 wt% solution is approximately 0.3 M even for a C_{18} soap), then the Stokes–Einstein relation [28] yields the hydrodynamic radius of the micelles to be of the order of 5.2 nm, assuming a zero-shear rate viscosity of 0.4665 mPa s for water at 60°C [29] and taking this as the viscosity of the continuous medium. The faster diffusing component approaches that of water at 60°C and may be associated with the diffusion of an alkyl-chain-containing species in solution. The fact that the fast diffusion coefficient can be resolved suggests that this species is not exchanging into and out of the micelles on the millisecond timescale of the PFG NMR measurement, which suggests a degree of phase separation, the origin of which is not clear. It is possible that the fast diffusing component includes dissolved monomer and/or glycerol present in the soap formulation.

The same isotropic soap solution was also studied by CYCLCROP edited PFG NMR using natural abundance ^{13}C. This method selectively detects the ^{1}H resonance of CH_2 in the alkyl chains of the soap molecules. For completeness, figure 3 shows an exemplar ^{13}C-edited spectra (in which the water signal has been completely suppressed). Each spectrum has been sensitized to self-diffusion to a different degree by increasing the PFG strength. The same figure shows the attenuation of the dominant peak in these spectra as a function of g^2. The solid line is a fit to the data according to the two-component diffusion model. The results are essentially identical to those of the normal ^{1}H experiment. The method has potential advantage when the water and soap resonance are poorly resolved such as in less dilute solutions or macroscopically inhomogeneous samples. However, it is expensive in experimental time and the signal-to-noise ratio of the data is nowhere near as good as standard ^{1}H PFG NMR.

Measurements of self-diffusion in equilibrated solutions at much lower water concentrations, where mesophases are expected, proved much harder due to the difficulty of preparing macroscopically homogeneous samples. Since samples could only be unambiguously characterized using ^2H_2O preparation and ^{2}H NMR, it was felt necessary to measure the diffusion of ^{2}H. Experiments gave $(8 \pm 1) \times 10^{-10} \, \text{m}^2 \, \text{s}^{-1}$ as characteristic of the diffusion coefficient of the anisotropic ^2H_2O associated with the hexagonal phase at water concentration between 30% and 60%. The diffusion coefficient varied little with water concentration within the uncertainties of the measurement within this range. For samples containing less than 50% water, a measure of the ^2H_2O diffusion coefficient in the lamellar phase could not be obtained. No attempt has been made to take into account the orientation of the liquid crystal nor has any attempt been made to narrow the liquid crystal NMR line and thereby improve the sensitivity of self-diffusion measurements in the mesophases [30].

4.4. ^{1}H MRI—conventional microscopy

Figure 4 shows two representative ^{1}H images recorded from a soap section exposed at the upper end to water. These two were recorded using an echo time of 4 ms after 40 min and 10 h of exposure respectively at 35°C. The brighter regions correspond to components with T_2 of the order of, or longer than, the echo time. These are the liquid water and mobile soap solution and some contribution from confined liquid and mobile chains. Neither solid soap nor mesophase ^{1}H are observed. The water ingress front is well delineated and is seen to advance down with time into the soap. However, beyond this quantitative feature, the images are rather bland and fail to reveal the complexity of the interface region.

4.5. ^{1}H MRI—stray field imaging

Figure 5(a) shows an example of unprocessed STRAFI echo-train data recorded across the developing soap bar/water interface for a section of commercial soap exposed to water at ambient temperature. This particular data set was collected 2 h after first exposure. It shows echo trains collected at each of 60 different sample positions spaced at 120 μm intervals. Each echo train comprises 128 echoes collected at $2\tau = 45 \, \mu$s intervals. The soap bar lies to the right and the water reservoir to the left, which was the top of the sample in the magnet. The initial position of the soap/water interface appears at 0 mm on the position axis.

The echo decay trains of figure 5(a) were first fit at every location to a single component exponential decay. The profiles shown in figure 5(b) were constructed from the decay amplitudes of this and other data sets. The single component fitting is clearly valid in the bulk water to the extreme left of the sample and gives a measure of water hydrogen density which can be normalized to unity. Elsewhere, the procedure yields the relative total hydrogen density excluding that hydrogen in the solid soap phases ($T_2 \approx 10 \, \mu$s; $2\tau = 45 \, \mu$s) to within a numerical factor corresponding to the different hydrogen density of water and soap. That this factor must be of the order of unity can be learnt by comparing the relative signal
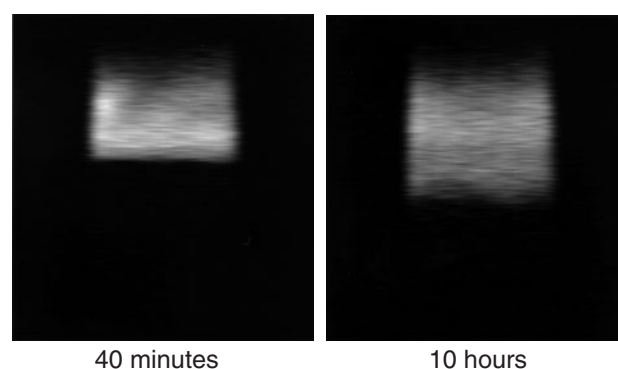

40 minutes   10 hours

Figure 4. Two magnetic resonance ^{1}H images of a soap section exposed to water at the upper end. The echo time was 4 ms, eliminating the short T_2 components so that the soap itself and mesophases are invisible (see table 1). The temperature was 35°C. The slice thickness was 2 mm and the in-plane resolution 39 μm × 625 μm. The two images were acquired 40 min and 10 h after initial exposure of the soap to water. The water may be seen to ingress the soap section with time.
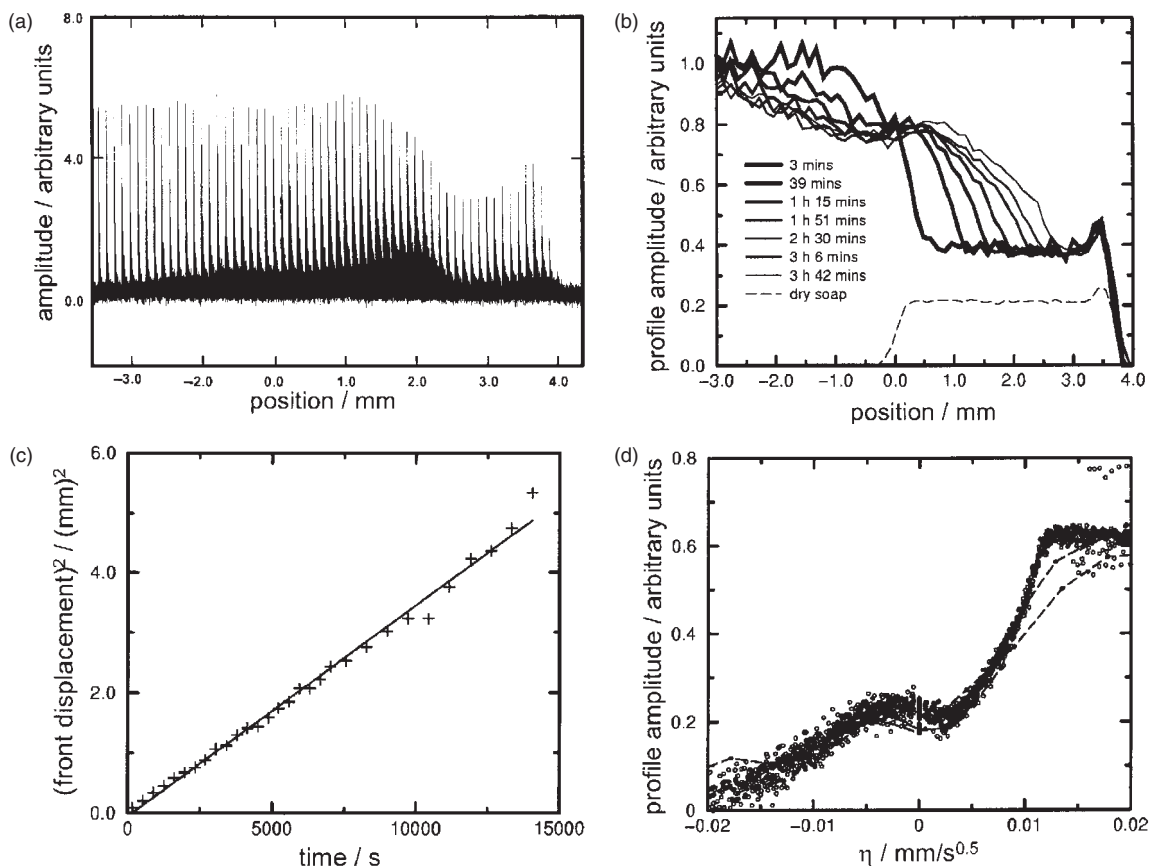
Figure 5. (*a*) Unprocessed STRAFI echo-train data recorded across the developing soap bar/water interface, 2 h after initial exposure to water of a commercial soap. The upper surface of the soap began at 0 mm on the position scale. Echo trains were recorded at each of 60 different sample positions separated by 120 μm. All are shown on the graph, which therefore represents a profile of the sample. At each sample position, 128 echoes were collected at 45 μs intervals. The soap bar lies to the right (positive displacement on the position axis) and the water reservoir to the left. (*b*) Selected profiles constructed from data such as that shown in figure 5(*a*) by plotting the amplitude of a single exponential fit to each echo decay. The amplitudes have been normalized to 1.0 in the water reservoir. The dry soap profile, before addition of the water reservoir, is shown as a dashed line, but the amplitudes cannot be directly compared as parameters were slightly altered in order to acquire the ingress data. (*c*) A graph of water front position squared versus time. The front position was arbitrarily chosen as that position where profile intensity reached 0.6. STRAFI profiles were acquired at 6 min intervals for the first 2 h and thereafter at 12 min intervals. The data are well represented by a straight line (———), which suggests that the diffusion process is broadly Fickian. (*d*) Profiles of solid soap density were constructed by subtracting the single exponential profiles (like those shown in 5(*b*)) from 1. This gives erroneous values below the soap section (where there is no water or semisolid soap); these data were discarded. The subtracted profiles were plotted against the reduced position parameter $\eta = z/(2t^{1/2})$. With the exception of the first two profiles (- - - -), there is a data collapse onto a master curve, which is indicative of a Fickian diffusion of solid soap into the water reservoir.

intensity from the STRAFI echo trains of mobile components within un-exposed soap ($\sim$0.4) and the expected intensity of 0.39 (17 + 7 + 15%) from table 1. Simple subtraction yields profiles of the solid soap density (except in the region below the soap core, position >3.5 mm). The subtraction method is the only practical way in which we can uniquely access the solid soap. A shorter value still of 2τ to substantially less than 10 μs would visualize the solid soap. However, the solid could not then be easily distinguished from the other components as all would be visualized. Additionally, quantitative contrast would be lost due to NMR spin locking [31], the smaller 2τ would appreciably lower the spatial resolution and the measurement would be very difficult.

Figure 5(*c*) shows a graph of the water ingress front position squared against time. The front position is arbitrarily taken as being at a profile intensity of 0.6. The plot is linear, from which it is inferred that diffusion process is Fickian [32]. The gradient of the plot yields a number which is

characteristic of the mutual diffusion coefficient for solid soap and soap solution. It is $(3.5 \pm 0.1) \times 10^{-10}$ m^2 s^{-1}. However, this overlooks the expected concentration dependence of the diffusivity.

The Fickian character of the diffusion process is exploited in figure 5(*d*) which shows the solid soap fraction, evaluated by subtraction as just described, of all the data recorded up to 4 h against the reduced position parameter $\eta = z/(2t^{1/2})$. All data, barring the first two profiles obtained (at 3 and 9 min, dashed lines), collapse onto a single curve. From this master curve it is, in principle, possible to extract the full concentration dependence of the mutual diffusion coefficient [32]. Although we have carried out this procedure, it relies on both differentiation and integration of the curve and the differentiation, in particular, introduced substantial noise and resulted in diffusivities of low significance.

The single exponential analysis misses the subtlety of the phase composition of the interfacial region. In order to access

the composition profiles for the more mobile components, and in particular the liquid crystal and confined liquid, it might be thought that it would be sensible to fit multi-exponential decays directly to the measured echo-train data of figure 5(*a*). In practice, this is fraught with difficulty and is less informative than might be imagined. The very shortest component (the solid soap) does not contribute greatly and is ignored. This leaves potentially three components based on relaxation measurements. However, the data do not warrant fitting to more than two relaxation components as now discussed. The results of a two-component exponential fitting to the echo decays are shown in figure 6. Figure 6(*a*) shows the component amplitudes and figure 6(*b*) shows the associated T_2 values for a single profile reconstructed from the raw data shown in figure 5(*a*), which was obtained 2 h after exposure of the soap section to water.

In the un-invaded, solid soap to the extreme right of the figure (position >3 mm), we find components of approximately equal intensity with T_2 values of 1 and 5 ms. These correspond roughly to the $\sim 100\,\mu s$ and liquid components (~ 1 and 10 ms), respectively, of the liquid crystal phase within the soap (table 1). Approaching the water

interface at 2 mm on the position scale, the proportion and T_2 of the longer component both dramatically increase, presumably due to an increase in both the mobility and abundance of the liquid components in the liquid crystal on swelling. Further up the sample, the T_2 value falls again as does the intensity. Well into the dilute region (water), <0 mm, the long component volume fraction is small and the T_2 value, although high, is very noisy. Turning now to the short component, the amplitude increases substantially in going from the soap through the interface to the water. The T_2 value also increases, but only slightly and it never exceeds 2 ms. Clearly at positions <0 mm, the long component cannot be ascribed to water which is the intuitive association. In fact, the very strong magnetic field gradient is causing substantial diffusion attenuation of the mobile component signals. The expected T_2^* of water in a gradient of $58\,T\,m^{-1}$ under a CPMG sequence with 2τ of $45\,\mu s$ is of the order of 2 ms [12] comparable to the *shorter value* (which corresponds to the *larger fraction*) in the solution region. The same diffusion attenuation is causing the decrease in the T_2 of the longer component in the intermediate region before the data becomes too noisy to be meaningful.

This crossover of T_2 components, with the short component representing *less mobile* components such as the liquid crystal in the soap and *more mobile* components in the water, poses significant difficulties for interpretation in the most interesting intermediate region. The crossover means that it is very difficult to obtain quantitative composition data about the dissolution interface from ^{1}H MRI based solely on T_2 contrast—whatever the pulse gap.

4.6. ^{2}H imaging and spatially resolved spectroscopy

The development of a non-equilibrium soap/water interfacial region was followed by ^{2}H MRI in one dimension (profiling). Figure 7 shows four ^{2}H profiles acquired 5 min, 2 h, 14 h and 3 days after exposure of the soap section to ^{2}H$_2$O. The soap itself was initially invisible, having been prepared with H$_2$O. Some exchange of ^{1}H in the soap with ^{2}H in the ^{2}H$_2$O is to
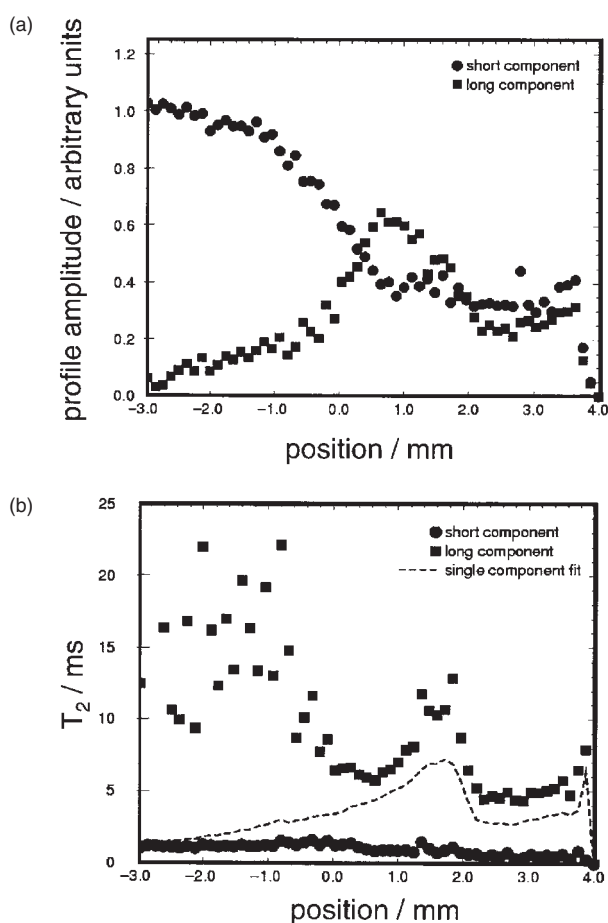

Figure 6. A single profile reconstructed from the raw data of figure 5(*a*) by fitting each echo train to two exponential components. The water reservoir lies to the left and the soap section to the right. The initial position of the soap surface was at 0 mm on the position axis. (*a*) The relative amplitudes of the two exponential components. (*b*) The relaxation time constant, T_2, values for the two exponential components.
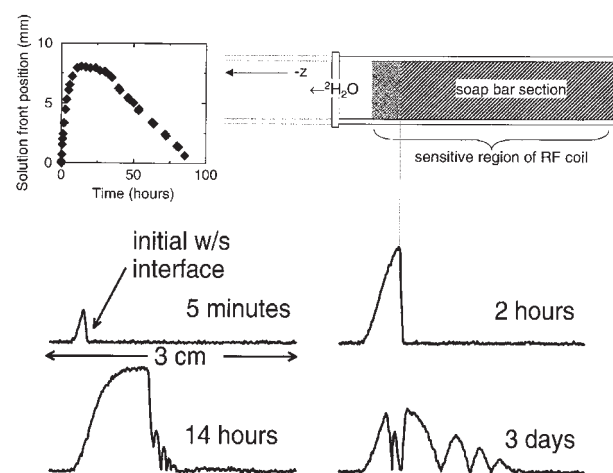

Figure 7. ^{2}H profiles of a developing soap/water interface at 5 min, 2 h, 14 h and 3 days. The schematic shows the sample presentation in the magnet. Profile amplitude is strongly attenuated outside the sensitive region of the RF coil, which eliminates much of the signal from the ^{2}H$_2$O reservoir. The echo time was 4 ms. The position of the isotropic solution front versus time is plotted in the inset graph.

be expected, certainly on a timescale of days. The more labile ^1H in the soap are in the water already present in the soap bar and exchange between ingressing ^2H_2O and water in the soap at the solvent front does not compromise the profiles. Exchange with the alkyl ^1H of the soap potentially leads to some signal attenuation, but is slow even on the timescale of these measurements. Attenuation of the signal from the ^2H_2O reservoir (to the left) was caused by the position of the soap/water interface at the extreme end of the RF sensor coil in order to maximize the volume of soap visualized. In the first 2 h, a sharp ^2H_2O front progressed steadily through the soap section. The signal was from isotropic ^2H. The ingress was qualitatively similar to that shown by the STRAFI measurements of figure 5(b). However, the echo time in the ^2H profiling was 4 ms, which eliminates the shortest T_2 components from the profile. Beyond 2 h, interpretation of the profiles became more complicated. The inset graph shows how the ^2H_2O front is eventually pushed back up the tube, by the swelling interfacial region. In addition, the profile contrast for the quadrupolar ^2H nucleus begins to reveal some of the phase complexity missing from the ^1H STRAFI data. The modulation of amplitude, which is apparent in both the 14 h and 3 day profiles below the ^2H_2O front, is caused by the quadrupolar splitting indicative of mesophase development. In this region, the phase evolution of spin 1 ^2H nuclei during the imaging pulse sequence results in a degree of signal cancellation depending on the particular value of $\Delta\nu_q$ at a given location [33, 34]. The varying profile modulation is indicative of a gradient in $\Delta\nu_q$ and hence water concentration along the length of the sample. It cannot be readily unfolded.

In order to obtain detailed information about the phase composition in the interfacial region, spatially localized, DQF spectra were obtained, in which the isotropic ^2H signal was suppressed. Only those ^2H with some anisotropy in their environment now contribute to the NMR signal. DQF spectra were obtained from 1 mm slices at regular intervals along the sample length. Positive distances are displacements into the soap sample, vertically downwards, $+z$, in accordance with the axis definition in figure 7. Figure 8(a) shows five DQF spectra from different slices obtained 4 days after exposure of the soap section to water. These spectra are assumed to represent mesophase domains which have no preferential orientation with respect to the applied magnetic field. Those equilibrated soap/water samples at water concentrations <50%, which showed reorientation effects in figure 2, took several hours to do so with temperature cycling. At water concentrations ⩾50%, powder-like spectra were obtained. The spectra of figure 8(a) are, therefore, antiphase powder-like spectra. A quadrupolar splitting, $\Delta\nu_q$, was measured between the outermost antiphase major peaks in these spectra. This figure was, therefore, a powder splitting for the hexagonal phase at water concentrations ⩾50% and a powder splitting for the lamellar phase at lower water concentrations. These splittings are both from domains with their principal quadrupolar axis oriented orthogonal to the magnetic field because they were measured between the major peaks of the powder spectrum. A single-valued calibration curve was therefore constructed using the values of $\Delta\nu_q$ given in figure 2 for the hexagonal phase (73% > water concentration ⩾ 50%) and half the values
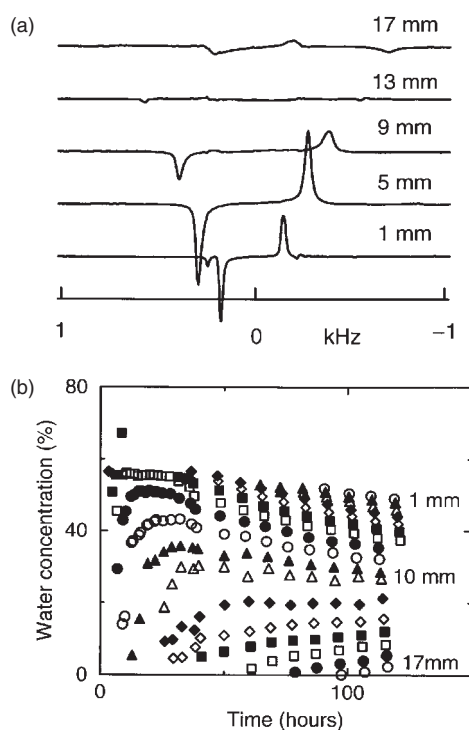

Figure 8. (a) Examples of spatially localized, DQF ^2H spectra obtained 4 days after initial exposure of the surface to ^2H_2O. The spectra arose from a selected 1 mm slice of the soap/water interface and were recorded with the pulse sequence of figure 1(d). The positions of the selected slices, with respect to the initial position of the soap surface, are indicated next to each spectrum. (b) A map of the change in water concentration with time in the soap/water interface region. These data were obtained by measurement of quadrupolar splittings from spectra such as those shown in figure 8(a) and conversion to water concentration through a calibration curve developed from figure 2 (see text).

of $\Delta\nu_q$ given in figure 2 for the reoriented lamellar phase (50% > water concentration ⩾ 25%). The calibration curve was extrapolated to lower values of water concentration which clearly exist in the macroscopically inhomogeneous samples. The calibration curve allowed the time evolution of the water concentration in the interface region to be evaluated from the time dependence of the spatially resolved DQF spectra. This evolution is shown in figure 8(b).

The data of figure 8(b) is reinterpreted in figure 9 as a more meaningful map of the developing mesophase distribution over the first 50 h of water ingress into the soap. The spatial resolution is 1 mm and temporal resolution is 1–2 h in the first 30 and 8–10 h thereafter. Water concentrations have been converted to mesophase identification based upon figure 2, with concentrations between 50% and 25% labelled as mixed hexagonal/lamellar liquid crystal, because a sharp hexagonal to lamellar phase boundary cannot be extracted from the data of figure 2. The first observation is of isotropic solution (L_1) above hexagonal liquid crystal (H_1) which develops at 3 mm from the origin. With time a further mixed layer of hexagonal/lamellar liquid crystal (H_1/L_α) develops. Eventually, after 32 h the leading layer is seen to be pure lamellar at a depth of 11 mm. The hexagonal liquid crystal stratum progresses to its furthest point from the initial interface position between 10 and 30 h after initial exposure. At this time
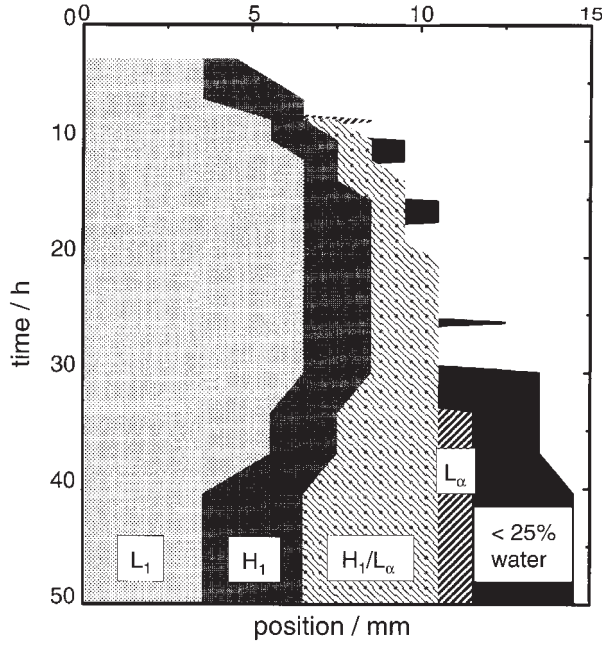
Figure 9. Reinterpretation of data from figure 8(*b*) as a map of developing mesophase distribution during the first 50 h of water ingress into the soap. The spatial resolution is 1 mm (determined by the thickness of the selected slice for each DQF spectrum) and the temporal resolution is about 1–2 h in the first 30 h and 8–10 h thereafter. For the shaded regions, $L_1 \equiv$ isotropic solution, $H_1 \equiv$ hexagonal mesophase, $L_\alpha \equiv$ lamellar mesophase. Solid black is uninvaded soap.

it invades 8 mm and is 1 mm thick. That the ingress apparently reverses is due entirely to the finite length of the sample (4 mm soap, 4 mm water this case) and the fact that the water diffusivity is strongly concentration dependent as explained below. This corresponds to the period on the inset graph in figure 7 when the isotropic ^{2}H$_2$O front appears stationary, after some ingress before being forced back up the tube.

4.7. Interface modelling

In order to model the phase evolution of the interface region, a one-dimensional Fickian diffusion process is assumed for which the governing equation is

$$\frac{\partial c}{\partial t} = \frac{\partial}{\partial z} D \frac{\partial c}{\partial z}, \qquad (2)$$

where c is the water concentration, z is position and t is time. The diffusion coefficient D is a single mutual diffusion coefficient describing the soap and water mixing. It is a strong function of c. Initially, D was considered as a two-valued function according to

$$\begin{aligned} D &= D_{\text{LC}}, \qquad c \leqslant 0.73, \\ &= D_{\text{IS}}, \qquad c > 0.73. \end{aligned} \qquad (3)$$

The initial conditions are $c = 0$, $L_1 < z < 0$ and $c = 1$, $0 < z < L_2$, where L_1 and L_2 are the extremes of the soap and water, respectively, and their initial interface lies at $z = 0$. The no-flux boundary condition was applied at both ends of the system.
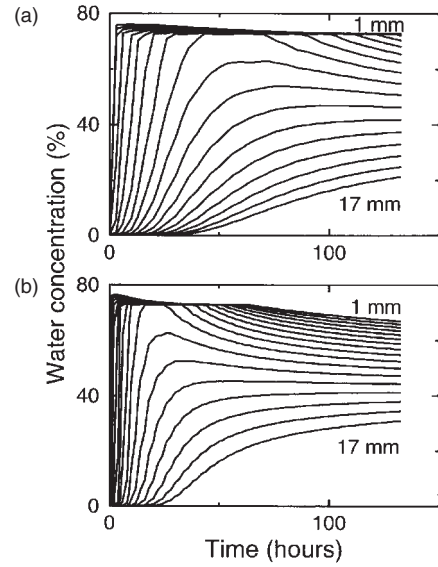
Figure 10. (*a*) A model of the evolution of water concentration in the soap/water interface region described in figure 8(*b*). The model was based upon equations (2) and (3), in which the mutual diffusion coefficient is considered as a two-valued function of concentration. (*b*) A second model according to equations (2) and (4), in which the mutual diffusion coefficient is assumed to have an exponential dependence upon concentration. Qualitative agreement with the data of figure 8(*b*) is reasonable.

Figure 10(*a*) shows an attempt to model the evolution of the interfacial region described by figure 8(*b*) using equations (2) and (3). The curves shown are evaluated using $D_{\text{IS}} = 8 \times 10^{-9} \text{ m}^2 \text{ s}^{-1}$ and $D_{\text{LC}} = 1 \times 10^{-10} \text{ m}^2 \text{ s}^{-1}$. By visual inspection, these values give the closest agreement with experiment. Closer agreement is obtained if both D_{IS} and D_{LC} are made dependent on concentration. An arbitrary exponential dependence is assumed.

$$\begin{aligned} D &= D_{\text{LC}} \exp\left(\frac{c}{c_0}\right), \qquad c \leqslant 0.73, \\ &= D_{\text{IS}} \exp\left(\frac{c}{c_1}\right), \qquad c > 0.73. \end{aligned} \qquad (4)$$

Figure 10(*b*) shows revised calculations using $D_{\text{IS}} = 2 \times 10^{-9} \text{ m}^2 \text{ s}^{-1}$, $c_0 = 0.3$, $D_{\text{LC}} = 5 \times 10^{-11} \text{ m}^2 \text{ s}^{-1}$ and $c_1 = 0.5$. The agreement with experiment is quite reasonable.

An independent estimate of D_{IS} has been gained from the results of the self-diffusion measurements already discussed. First a self-diffusion coefficient for the soap is estimated by combining D_1 and D_2 according to

$$\frac{1}{D_{\text{soap}}} = \frac{a_1}{D_1} + \frac{a_2}{D_2}, \qquad (5)$$

where a_1 and a_2 are the normalized amplitudes of the two components. The composite self-diffusion coefficient is then combined with that of the water to yield the mutual diffusion coefficient [35]:

$$D_{\text{IS}} = c(D_{\text{soap}} - D_{\text{water}}) + D_{\text{water}}. \qquad (6)$$

It was found that D_{IS} was of the order of $1 \times 10^{-9} \text{ m}^2 \text{ s}^{-1}$. This is about an order of magnitude smaller than used in the spatial data fitting.

The same procedure was attempted using equilibrated samples of liquid crystal in order to estimate the mutual diffusion coefficient D for $c < 0.73$. An indicative value of 1×10^{-10} cm^2 s^{-1} for D_{LC} was obtained, though the uncertainty was large. However, this is in better agreement with the spatial measurement fitting than the value of D_{IS}.

5. Conclusions

A quantitative description of the developing soap/water interfacial region was derived from a series of spatially resolved NMR measurements. [1]H STRAFI was employed to give a simplistic description of water ingress into an intact soap bar, but the T_2 contrast in this measurement was insufficient to detail the developing mesophases in the interfacial region, despite the fact that the different phases are known to have different spin–spin relaxation time constants. DQF profiling of a soap/heavy water interface allowed the signal from isotropic solution to be suppressed and the spatial distribution of liquid crystalline mesophases (and, hence, water concentration) to be studied in the light of calibration DQF measurements on soap solutions of known composition. The DQF methods allowed a far more complete picture of mesophase formation in the interfacial region to be quantified than did the simple ^{1}H STRAFI profiling. The DQF measure of water concentration (figure 8(b)) is independent of relaxation time, being instead derived from the quadrupolar splitting in the ^{2}H spectrum. A simple model of the mutual diffusion process is in good qualitative agreement with these data. The DQF is a useful tool in removing the contribution of isotropic soap solution and [2]H$_2$O, but that solution is a further component of the developing soap/water interface. PFG measurements in soap solution give an estimate of micelle size ($\sim$5 nm) in the isotropic fluid above the interfacial region. Normal PFG measurements and measurements by a combination of PFG and CYCLCROP (which is highly chemically selective for the alkyl ^{1}H of the soaps) were in very good agreement.

Acknowledgments

References

[1] Gerritson H C and Caffrey M 1990 *J. Phys. Chem.* **94** 944–8
[2] Gray G W 1962 *Molecular Structures and the Properties of Liquid Crystals* (London: Academic)
[3] Sackmann H and Demus D 1973 *Mol. Cryst. Liq.Cryst.* **21** 239–73
[4] Saupe A and Englert G 1963 *Phys. Rev. Lett.* **11** 462–4
[5] Dong R Y 1997 *Nuclear Magnetic Resonance of Liquid Crystals* 2nd edn (New York: Springer)
[6] Wade C G 1977 *Annu. Rev. Phys. Chem.* **28** 47–73
[7] Roeder S B W, Burnell E E, Kuo A and Wade C G 1976 *J. Chem. Phys.* **64** 1848–9
[8] Lindblom G and Orädd G 1994 *Prog. Nucl. Magn. Reson. Spectrosc.* **26** 483–515
[9] Meiboom S and Gill D 1958 *Rev. Sci. Intstrum.* **29** 688–91
[10] Bevington P R 1969 *Data Reduction and Error Analysis for the Physical Sciences* 1st edn (New York: McGraw-Hill) chapter 11
[11] Tanner J E 1970 *J. Chem. Phys.* **52** 2523
[12] Callaghan P T 1991 *Principles of Nuclear Magnetic Resonance Microscopy* 1st edn (Oxford: Oxford University Press) chapter 3
[13] Kunze C and Kimmich R 1994 *J. Magn. Reson. B* **105** 38
[14] Chandrakumar N and Kimmich R 1999 *J. Magn. Reson.* **137** 100–7
[15] Samoilenko A A 1987 *Z. Fiz. Kh.* **61** 3082–5
[16] McDonald P J and Newling B 1998 *Rep. Prog. Phys.* **61** 1441–93
[17] Nunes T, Randall E W, Samoilenko A A, Bodart P and Feio G 1996 *J. Phys. D: Appl. Phys.* **29** 805–8
[18] Prado P J, Balcom B J, Beyea S D, Bremner T W, Armstrong R L, Pishe R and Gratten-Bellew P E 1998 *J. Phys. D: Appl. Phys.* **31** 2040–50
[19] Cottrell S P, Halse M R and Strange J H 1990 *Meas. Sci. Technol.* **1** 624–9
[20] Tsoref L, Shinar H, Seo Y, Eliav U and Navon G 1998 *Magn. Reson. Med.* **40** 720–6
[21] McBain J W and Sierichs Wm C 1948 *J. Am. Oil Chemists' Soc.* **25** 221–5
[22] Clayden N J and Hesler B D 1992 *J. Magn. Reson.* **98** 271–82
[23] Skoulios A 1967 *Adv. Colloid Int. Sci.* **1** 79–110
[24] Westlund P O 2000 *J. Phys. Chem. B* **104** 6059–64
  Takahashi A, Takizawa T and Nakata Y 1989 *Chem. Phys. Lett.* **163** 65–8
[25] Burgoyne J, Holmes M C and Tiddy G J T 1995 *J. Phys. Chem.* **99** 6054–63
[26] Holz M, Heil S R and Sacco A (ed) 2000 4.748×10^{-9} m^2 s^{-1} in *Bruker Almanac 2001, Phys. Chem. Chem. Phys.* **2** 4740–2
[27] Aniansson G E A 1985 *Prog. Colloid Polym. Sci.* **70** 2–5
[28] Bird R B, Stewart W E and Lightfoot E N 1960 *Transport Phenomena* 1st edn (New York: Wiley) chapter 16
[29] Lide D R (ed) 1999 *CRC Handbook of Physics & Chemistry* 80th edn (New York: CRC Press) chapter 6
[30] Chang I, Hinze G, Diezemann G, Fujara F and Sillescu H 1996 *Phys. Rev. Lett.* **76** 2523–6
[31] Ostroff E D and Waugh J S 1966 *Phys. Rev. Lett.* **16** 1097–8
[32] Crank J 1975 *The Mathematics of Diffusion* 2nd edn (Oxford: Oxford University Press) chapter 2
[33] Dixon W T 1984 *Radiology* **153** 189–94
[34] Glover G H and Schneider E 1991 *Magn. Reson. Med.* **18** 371–83
[35] Crank J 1975 *The Mathematics of Diffusion* 2nd edn (Oxford: Oxford University Press) chapter 10